INTERNATIONAL JOURNAL OF NUMERICAL MODELLING: ELECTRONIC NETWORKS, DEVICES AND FIELDS
Int. J. Numer. Model. 2001; **14**:31–47

Forcing term discretization techniques in the external field-to-MTL coupling problems

Tibor Lapohos[1,*,†] and Joe LoVetri[2]

[1]*Defence Research Establishment Ottawa, Electronic Countermeasures, 3701 Carling Ave., Ottawa, ON, Canada K1A 0K2*
[2]*Department of Electrical and Computer Engineering, University of Manitoba, Winnipeg, MB, Canada R3T 5V6*

SUMMARY

In this paper, two, under certain conditions, equivalent models of electromagnetic plane wave coupling to multiconductor transmission lines (MTLs) are described. The 'frequency-to-time domain' (FTD) model incorporates the effect of the impinging electromagnetic waves by means of distributed voltage and current sources whose expressions are found through mathematical approximations made in the frequency domain followed by a transformation to the time domain. The approximations were made in order to gain an advantage in computation time in the discrete FTD (DFTD) model. In contrast to this approach, the same distributed sources of the 'approximate analytic' (AA) model are derived by directly evaluating the corresponding integral formulas. It is shown that, although the same second-order-accurate discretization technique has been employed to create both the DFTD and the discrete AA (DAA) models, the simulation results are not the same. In the case of the DFTD model, significant numerical error can be seen in the simulation results, whereas the DAA model does not show such a behaviour. It is shown that time averaging of the forcing terms in the DFTD model helps to reduce the numerical errors significantly at no extra computational cost. Copyright © 2001 Crown in the right of Canada. Published by John Wiley & Sons, Ltd.

KEY WORDS: multiconductor transmission lines; MTL; external field coupling; numerical simulation; discretization techniques; forcing terms

1. INTRODUCTION

Assuming the quasi-TEM mode of propagation, in terms of total voltages, the $m + 1$ conductor multiconductor transmission line (MTL) depicted in Figure 1 is modelled by the following partial differential equations [1]:

$$\begin{aligned} \frac{\partial}{\partial y}\mathbf{V}(t, y) + L\frac{\partial}{\partial t}\mathbf{I}(t, y) + R\mathbf{I}(t, y) &= \mathbf{V}_{\mathrm{f}}(t, y) \\ \frac{\partial}{\partial y}\mathbf{I}(t, y) + C\frac{\partial}{\partial t}\mathbf{V}(t, y) + G\mathbf{V}(t, y) &= \mathbf{I}_{\mathrm{f}}(t, y) \end{aligned} \tag{1}$$

*Correspondence to: Tibor Lapohos, Defence Research Establishment Ottawa, Electronic Countermeasures, 3701 Carling Ave., Ottawa, Ontario, Canada K1A 0K2.
† E-mail: tibor.lapohos@ieee.org

Received 3 December 1998
Revised 12 July 1999

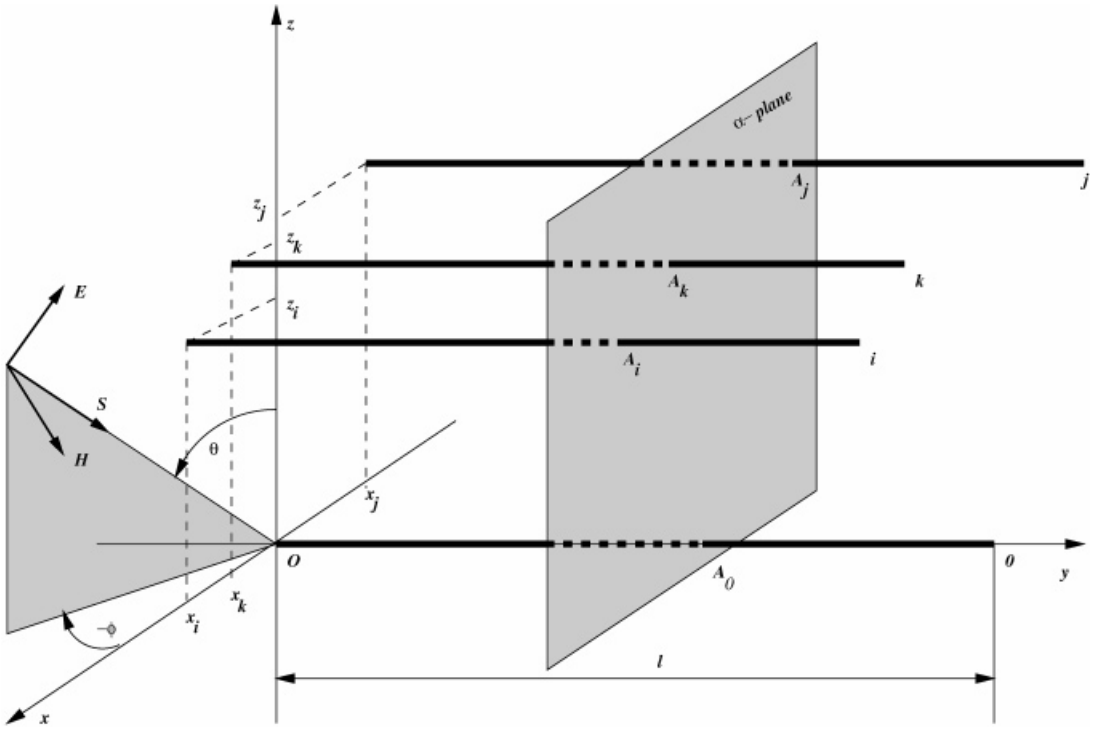

Figure 1. Multiconductor transmission line illuminated by an external electromagnetic field.

where the $m \times m$ per-unit-length (PUL) inductance and capacitance matrices, L and C, are known or estimated parameters. The $m \times 1$ total voltage and current column vectors, $\mathbf{V}(t, y)$ and $\mathbf{I}(t, y)$, are the unknowns which are to be solved. The forcing functions, which are due to the external field coupling to the MTL, are the induced voltage density, $\mathbf{V}_{\mathrm{f}}(t, y)$, and the induced current density, $\mathbf{I}_{\mathrm{f}}(t, y)$. In terms of the incident electric field, $\mathbf{E}^{\mathrm{i}}$, these can be expressed as [1–4]

$$\mathbf{V}_{\mathrm{f}}(t, y) = \begin{bmatrix} \cdots \\ -\dfrac{\partial}{\partial y}\displaystyle\int_{A_0}^{A_j} \mathbf{E}_t^{\mathrm{i}} \cdot \mathrm{d}\mathbf{l} + \mathbf{E}_y^{\mathrm{i}}(t, x_j, y, z_j) - \mathbf{E}_y^{\mathrm{i}}(t, 0, y, 0) \\ \cdots \end{bmatrix}$$

$$\mathbf{I}_{\mathrm{f}}(t, y) = -G \begin{bmatrix} \cdots \\ \displaystyle\int_{A_0}^{A_j} \mathbf{E}_t^{\mathrm{i}} \cdot \mathrm{d}\mathbf{l} \\ \cdots \end{bmatrix} - C \frac{\partial}{\partial t} \begin{bmatrix} \cdots \\ \displaystyle\int_{A_0}^{A_j} \mathbf{E}_t^{\mathrm{i}} \cdot \mathrm{d}\mathbf{l} \\ \cdots \end{bmatrix} \tag{2}$$

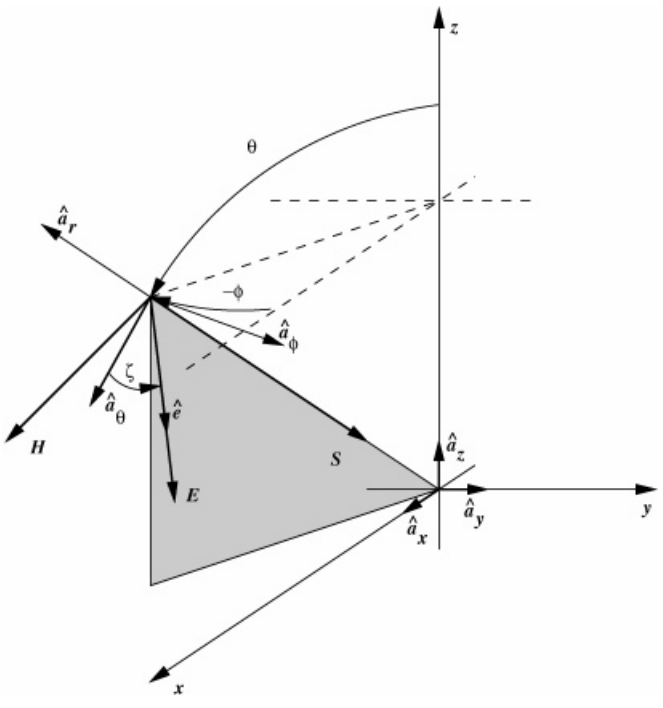

Figure 2. Specification of the incident electromagnetic wave.

In the line integral terms, A_j denotes the point in which the α-plane, which is perpendicular to the y-axis, intersects the jth line of the MTL. The α-plane intersects the y-axis, which is co-linear with the reference conductor 0, at the point A_0 whose co-ordinates are $(0, y, 0)$. In (2), $\mathbf{E}_t^{\mathrm{i}}$ denotes the transverse component of the incident electric field intensity vector; that is the projection of $\mathbf{E}^{\mathrm{i}}$ onto the α-plane. The longitudinal component of the incident electric field is denoted by $\mathbf{E}_y^{\mathrm{i}}$.

In practice, MTLs are usually terminated by complicated non-linear circuits and a system of MTLs having junctions of such circuits form a non-linear MTL network. In order to simulate such MTL networks, we employ [5–7] the popular modified nodal analysis (MNA) formulation at the non-linear junctions (this is the formulation used in SPICE). For the case of a single MTL with linear terminations, one of the two scattered field formulations described in References [3,4] prove to be more efficient than the total field formulation. Unfortunately, a method of combining the scattered field formulation with the MNA description of non-linear junctions in an MTL network is not known. Therefore, we use the total field formulation for the coupling of electromagnetic fields to the MTLs where no such problem exists.

The specification of the incident plane wave is shown in Figure 2, where we denote the unit vectors of the spherical co-ordinate system as $\hat{a}_r$, $\hat{a}_\theta$ and $\hat{a}_\phi$. As can be seen in the figure, the direction of propagation $-\hat{a}_r$ of the incident electromagnetic plane wave is specified by the angles θ and ϕ, whereas the polarization is specified by the angle ζ of the electric field vector $\mathbf{E}^{\mathrm{i}}$ being measured from $\hat{a}_\theta$ towards $\hat{a}_\phi$. Since the medium outside the MTL is being assumed to be free space, characterized by μ_{o} and ε_{o}, the plane wave propagates with a speed of $v_{\mathrm{o}} = (\mu_{\mathrm{o}}, \varepsilon_{\mathrm{o}})^{-1/2}$.

In the Cartesian co-ordinate system of Figure 2, denoting the unit vectors as $\hat{a}_x$, $\hat{a}_y$ and $\hat{a}_z$, the incident plane wave can be specified as

$$\mathbf{E}^{\mathrm{i}}(t, \mathbf{r}) = \hat{\mathbf{e}} E_{\mathrm{o}}(t - \mathbf{v} \cdot \mathbf{r}/|\mathbf{v}|^2) \tag{3}$$

where $\mathbf{r} = x\hat{a}_x + y\hat{a}_y + z\hat{a}_z$ is the position vector, t is the time, and $\hat{\mathbf{e}}$ is the unit vector specifying the direction of the electric field, and $E_{\mathrm{o}}(\cdot)$ is the electric field waveform function. In terms of the parameters described above, this unit vector $\hat{\mathbf{e}}$ can be written as,

$$\hat{\mathbf{e}} = e_x\hat{a}_x + e_y\hat{a}_y + e_z\hat{a}_z = \cos(\zeta)\hat{a}_\theta + \sin(\zeta)\hat{a}_\phi = [0 \quad \cos\zeta \quad \sin\zeta]\, R_{\mathrm{sph}}\, [\hat{a}_x \quad \hat{a}_y \quad \hat{a}_z]^{\mathrm{T}} \tag{4}$$

where R_{sph} denotes the transformation matrix between the spherical and Cartesian co-ordinate systems:

$$R_{\mathrm{sph}} = \begin{bmatrix} \sin\theta\cos\phi & \sin\theta\sin\phi & \cos\theta \\ \cos\theta\cos\phi & \cos\theta\sin\phi & -\sin\theta \\ -\sin\phi & \cos\phi & 0 \end{bmatrix} \tag{5}$$

From this it follows that, in Cartesian co-ordinates, the direction of the incident electric field can be written as

$$\hat{\mathbf{e}} = [\cos\theta\cos\phi\cos\zeta - \sin\phi\sin\zeta \quad \cos\theta\sin\phi\cos\zeta + \cos\phi\sin\zeta \quad -\sin\theta\cos\zeta]\, [\hat{a}_x \quad \hat{a}_y \quad \hat{a}_z]^{\mathrm{T}} \tag{6}$$

The velocity vector of the wave can also be written in Cartesian co-ordinates as,

$$\mathbf{v} = v_x\hat{a}_x + v_y\hat{a}_y + v_z\hat{a}_z = -v_{\mathrm{o}}\hat{a}_r = [-v_{\mathrm{o}} \quad 0 \quad 0]\, R_{\mathrm{sph}}\, [\hat{a}_x \quad \hat{a}_y \quad \hat{a}_z]^{\mathrm{T}} \tag{7}$$

that is

$$\mathbf{v} = [-v_{\mathrm{o}}\sin\theta\cos\phi \quad -v_{\mathrm{o}}\sin\theta\sin\phi \quad -v_{\mathrm{o}}\cos\theta]\, [\hat{a}_x \quad \hat{a}_y \quad \hat{a}_z]^{\mathrm{T}} \tag{8}$$

With the exception of some boundary conditions, which describe the electrical terminal conditions of the MTL, equations (1)–(3), (6) and (8) complete the mathematical model of the physical problem we are interested in. This mathematical model must be solved numerically and in this paper we consider the standard second-order-accurate interlaced leap-frog scheme for the solution of the MTL partial differential equations:

$$\begin{aligned} \mathbf{I}_{k+1/2}^{n+1/2} &= \left[\Delta y\left(\frac{L}{\Delta t} + \frac{R}{2}\right)\right]^{-1}\left[\Delta y\left(\frac{L}{\Delta t} - \frac{R}{2}\right)\mathbf{I}_{k+1/2}^{n-1/2} - \mathbf{V}_{k+1}^{n} + \mathbf{V}_{k}^{n} + \Delta y[\mathbf{V}_{\mathrm{f}}]_{k+1/2}^{n}\right] \\ \mathbf{V}_{k}^{n+1} &= \left[\Delta y\left(\frac{C}{\Delta t} + \frac{G}{2}\right)\right]^{-1}\left[\Delta y\left(\frac{C}{\Delta t} - \frac{G}{2}\right)\mathbf{V}_{k}^{n} - \mathbf{I}_{k+1/2}^{n+1} + \mathbf{I}_{k-1/2}^{n+1/2} + \Delta y[\mathbf{I}_{\mathrm{f}}]_{k}^{n+1/2}\right] \end{aligned} \tag{9}$$

The voltage, $\mathbf{V}_k^n \approx \mathbf{V}(n\Delta t, k\Delta y)$, and the current, $\mathbf{I}_{k+1/2}^{n-1/2} \approx \mathbf{I}((n-1/2)\Delta t, (k+1/2)\Delta y)$, vectors are interlaced in space and time. The derivation of this computationally efficient numerical scheme

has been described in Reference [1]. In the following section, we present two methods to discretize the forcing functions $[\mathbf{V}_f]_{k+1/2}^n$ and $[\mathbf{I}_f]_k^{n+1/2}$.

2. APPROXIMATE MODELS

If the illuminating field is plane wave, it is possible to find a simple form for the distributed voltage and current sources of (2). If the external field is not a plane wave, the problem becomes more complex, but still treatable by numerical methods. Several researchers have evaluated the distributed sources for a transmission line (TL) embedded in an inhomogeneous medium when illuminated by an external field [8–11]. The perturbation of the incident field by the dielectric medium is often assumed to be negligible and thus ignored. It has been found in Reference [6] that for the case of a plane wave impinging on an MTL embedded in an inhomogeneous dielectric medium, the perturbation of the incident field due to the dielectric must be included for a correct solution of the problem. The same ideas are reflected in References [12,13].

In the following two sections, approximate models are described for modelling plane waves impinging on MTLs embedded in strictly homogeneous media. The numerical details of these models are studied since they form the basis for extending the analysis to the case of MTLs immersed in a heterogeneous dielectric medium. In Section 2.1, a new discretization procedure is presented which is more accurate than the more common technique described in Section 2.2 (see also Reference [1]). Finally, in Section 2.3, the formulations of the two approximate models are compared. Numerical experiments are also presented to validate the arguments.

2.1. Analytic-approximate (AA) models

One way to determine an explicit formula for the forcing functions $\mathbf{V}_f(t, y)$ and $\mathbf{I}_f(t, y)$ is to substitute the functional form of the plane wave into Equation (2) and analytically evaluate the integral terms therein. After the considerable simplification given in the appendix of Reference [14], we find that

$$\mathbf{V}_f(t, y) = \begin{bmatrix} \cdots \\ \left(\dfrac{f_j}{g_j} v_y - e_y\right) E_d(t, y, g_j/v_o^2) \\ \cdots \end{bmatrix}$$

$$\mathbf{I}_f(t, y) = -C \begin{bmatrix} \cdots \\ \dfrac{f_j}{g_j} v_o^2 E_d(t, y, g_j/v_o^2) \\ \cdots \end{bmatrix} \tag{10}$$

where the notation

$$\begin{aligned} f_j &= e_x x_j + e_z z_j \\ g_j &= v_x x_j + v_z z_j \end{aligned} \tag{11}$$

and

$$E_{\mathrm{d}}(t, y, \tau) = E_{\mathrm{o}}(t - v_y y/v_{\mathrm{o}}^2) - E_{\mathrm{o}}(t - \tau - v_y y/v_{\mathrm{o}}^2)$$
$$\tau = g_j/v_{\mathrm{o}}^2 \quad \text{(s)} \tag{12}$$

has been introduced to simplify the expressions. From Equation (10) we see that all elements of the forcing functions $\mathbf{V}_{\mathrm{f}}(t, y)$ and $\mathbf{I}_{\mathrm{f}}(t, y)$ are directly proportional to the difference in the intensity of the electric field at the corresponding conductor and at the reference conductor at appropriate instants of time. Hereafter we refer to the group of equations [(1), (10)–(12)] as the *analytic-approximate* (AA) model of our problem.

In (12), τ is the time it takes for the plane wave to travel from the jth conductor to the reference conductor. We remark that no approximations have been made in the derivation from Equations (2)–(10). The only approximation that will be made is in terms of the discretization procedure which will now be described.

As required by Equation (9), the *discrete* model of the problem (1), the forcing functions given by (10) have to be discretized so that $[\mathbf{V}_{\mathrm{f}}]_{k+1/2}^{n}$ and $[\mathbf{I}_{\mathrm{f}}]_{k}^{n+1/2}$ are obtained. Thus, the distributed voltage forcing function is discretized by using centred differencing at integer time and half spatial locations, whereas the distributed current forcing function is discretized at half time and integer spatial locations:

$$[\mathbf{V}_{\mathrm{f}}]_{k+1/2}^{n} = \begin{bmatrix} \cdots \\ \left(\dfrac{f_j}{g_j} v_y - e_y\right)[E_{\mathrm{d}j}]_{k+1/2}^{n} \\ \cdots \end{bmatrix}$$
$$[\mathbf{I}_{\mathrm{f}}]_{k}^{n+1/2} = -C \begin{bmatrix} \cdots \\ \dfrac{f_j}{g_j} v_{\mathrm{o}}^2 [E_{\mathrm{d}j}]_{k}^{n+1/2} \\ \cdots \end{bmatrix} \tag{13}$$

where the notation

$$[E_{\mathrm{d}j}]_{k}^{n} = E_{\mathrm{d}j}(n\Delta t, k\Delta y, g_j/v_{\mathrm{o}}^2)$$

has been used. We denote the approach of using the discrete forcing functions given by Equation (13) as the *discrete* analytic-approximate (DAA) model.

As it is written in (13), the DAA solution produces high-frequency numerical oscillations around the true solution. An example of such oscillations is presented in our numerical study (see Section 3). In order to add damping to the numerical scheme, time averaging is used in the source terms. Hence, from (13) we obtain,

$$[\mathbf{V}_{\mathrm{f}}]_{k+1/2}^{n} = \begin{bmatrix} \cdots \\ \left(\dfrac{f_j}{g_j} v_y - e_y\right) \dfrac{[E_{\mathrm{d}j}]_{k+1/2}^{n+1/2} + [E_{\mathrm{d}j}]_{k+1/2}^{n-1/2}}{2} \\ \cdots \end{bmatrix} \tag{14}$$

$$[\mathbf{I}_\mathrm{f}]_k^{n+1/2} = -C\begin{bmatrix} \cdots \\ \dfrac{f_j}{g_j}\, v_\mathrm{o}^2 \dfrac{[E_{\mathrm{d}j}]_k^{n+1} + [E_{\mathrm{d}j}]_k^n}{2} \\ \cdots \end{bmatrix}$$

to which, in the rest of this work, we refer as the *averaged-source* DAA (ADAA) model.

The time averaging has to be carried out for each element of the $[\mathbf{V}_\mathrm{f}]_{k+1/2}^n$ and $[\mathbf{I}_\mathrm{f}]_k^{n+1/2}$ vectors. Since the $E_\mathrm{d}(t, y, \tau)$ function is a difference function, the computational cost of the time varying part of (14) for each forcing function consists basically of two subtraction, one addition and one multiplication operation for each conductor since the factors $(f_j v_y/g_j - e_y)/2$ and $f_j v_0^2/(2g_j)$ do not depend on time and can be calculated before the time iteration starts. Thus, this scheme requires four floating point operations for each conductor and for each forcing function, that is $8 \times m$ floating point operations for the MTL.

2.2. Frequency-to-time domain (FTD) models

An alternative approach is to first convert the original forcing functions $\mathbf{V}_\mathrm{f}(t, y)$ and $\mathbf{I}_\mathrm{f}(t, y)$ to the phasor domain, carry out some analytic manipulations making some approximations based on the wavelength as compared to the distance between conductors, and subsequently convert back to the time domain. The complete procedure is described in Reference [1] and, employing the present notation, the approximate *frequency-to-time domain* (FDT) forcing functions can be written down as

$$\begin{aligned} \mathbf{V}_\mathrm{f}(t, y) &= \begin{bmatrix} \cdots \\ \left(\dfrac{f_j}{g_j}\, v_y - e_y\right)\dfrac{g_j}{v_\mathrm{o}^2} \\ \cdots \end{bmatrix} \frac{\partial}{\partial t}\, E_\mathrm{o}(t - v_y y/v_\mathrm{o}^2) \\ \mathbf{I}_\mathrm{f}(t, y) &= -C\begin{bmatrix} \cdots \\ f_j \\ \cdots \end{bmatrix} \frac{\partial}{\partial t}\, E_\mathrm{o}(t - v_y y/v_\mathrm{o}^2) \end{aligned} \tag{15}$$

In order to obtain these formulas, the approximation

$$\begin{aligned} \frac{\sin \Psi_j}{\Psi_j}\, \mathrm{e}^{-\mathrm{i}\Psi_j} &\approx 1, \quad \forall j \\ \Psi_j = \frac{v_x x_j + v_z z_j}{2} &= \frac{g_j}{2v_\mathrm{o}^2}\, \omega = \frac{g_j}{\lambda v_\mathrm{o}}\, \pi \end{aligned} \tag{16}$$

has been made. Hence, Ψ_j must be small in order for this approximation to be applicable. This approximation restricts the method to MTLs with small cross-sectional size as compared to the wavelength of the incident impinging wave; quite a valid assumption considering that the same restriction applies to the use of the quasi-TEM formulation of the MTL equations in the first

place! Hereafter, we refer to the set of equations [(1), (15) and (16)] as the *frequency-to-time domain* (FTD) model of our field coupling problem.

The FTD forcing functions, given by (15), are now discretized using a second-order-accurate finite difference scheme, as was done in the AA formulation, to arrive at the discrete form forcing functions:

$$[\mathbf{V}_\mathrm{f}]_{k+1/2}^{n} = \begin{bmatrix} \cdots \\ \left(\dfrac{f_j}{g_j} v_y - e_y\right)\dfrac{g_j}{v_\mathrm{o}^2} \\ \cdots \end{bmatrix} \frac{[E_\mathrm{a}]_{k+1/2}^{n+1/2} - [E_\mathrm{a}]_{k+1/2}^{n-1/2}}{\Delta t}$$

$$[\mathbf{I}_\mathrm{f}]_{k}^{n+1/2} = -C \begin{bmatrix} \cdots \\ f_j \\ \cdots \end{bmatrix} \frac{[E_\mathrm{a}]_{k}^{n+1} - [E_\mathrm{a}]_{k}^{n}}{\Delta t} \tag{17}$$

where

$$[E_\mathrm{a}]_k^n = E_\mathrm{o}(n\Delta t - v_y k \Delta y / v_\mathrm{o}^2)$$

In the rest of the work we refer to (17) as the forcing function of the *discrete* FTD (DFTD) model.

It is now easy to see that, in this case, the computational cost of the time-varying terms for each of the forcing functions consists of only one subtraction for the whole MTL and one multiplication for each conductor, that is $2 \times (m + 1)$ floating point operations. As before, the factors $g_j(f_j v_y/g_j - e_y)/(\Delta t v_\mathrm{o}^2)$ and $f_j/\Delta t$ are independent of time. This formulation is more computationally efficient than the ADAA formulation, which is the only advantage of the FTD model over the AA model.

2.3. Comparison of FTD and AA models

Comparing the forcing functions of the AA and FTD models, given by Equations (10) and (15), we find that if the partial derivative term in (15) is approximated by

$$\frac{\partial}{\partial t} E_\mathrm{o}(t - v_y y/v_\mathrm{o}^2) \approx \frac{E_\mathrm{o}(t - v_y y/v_\mathrm{o}^2) - E_\mathrm{o}(t - v_y y/v_\mathrm{o}^2 - \Delta t)}{\Delta t} \tag{18}$$

and the time step Δt is chosen the same as the time it takes the wave to travel from the jth conductor to the reference conductor, that is,

$$\Delta t = \tau = g_j / v_\mathrm{o}^2, \tag{19}$$

then the jth element of both forcing functions given by (15) become exact expressions, vis-a-vis equation (10). Therefore, (18) and (19) constitute the basic relationship between the AA and FTD models. Any different value of Δt than g_j/v_o^2 can cause significant inaccuracies. Of course, it is impossible to choose a Δt which makes all terms exact, since for each conductor g_j is different. That is, one can replace Δt in (17) separately for each one of the conductors with the appropriate value dictated by (19), but then the DFTD model becomes the same as the DAA model, hence

losing its computational advantage. We find it important to underline that, when talking about the approximations of the source terms given by (15), the required Δt in (18), or (17) as a matter of fact, can be different from the best possible time step which could be used in (9) in order to obtain the least amount of numerical dispersion.

For example, it is well known that, in order to obtain the least amount of numerical dispersion, the leap-frog scheme should be run with a time step equal to the maximum time step allowed by the Courant stability limit, i.e. $\Delta t = \Delta x / v_{\max}$, where $v_{\max}$ is the maximum modal-speed on the MTL. From this, using (19), we see that for minimum dispersion we require

$$\Delta x = \tau v_{\max} = d_{\text{eff}} \frac{v_{\max}}{v_{\text{o}}} \tag{20}$$

where $d_{\text{eff}} = \tau v_{\text{o}}$ is the effective cross-sectional distance between the conductors. For a transmission line in free space we have $v_{\max} = v_{\text{o}}$ and thus we see that satisfying (19) implies setting $\Delta x = d_{\text{eff}}$. This may be a much smaller value than that required for resolving the shortest wavelength, λ_{c}, and this will result in an inefficient use of computer resources. If, on the other hand, we set $\Delta x = \lambda_{\text{c}}/10 \neq d_{\text{eff}}$, then we violate condition (19).

3. NUMERICAL ANALYSIS

We incorporated the two types of forcing functions, i.e. ADAA and DFTD, into the same numerical algorithm containing the interlaced leapfrog scheme in order to solve the same problems. We considered three- and two-conductor transmission lines, with and without ground planes, and varied the incident plane wave in terms of its angle of incidence θ and ϕ. We found that the solutions obtained with the two kinds of forcing functions agreed very well, except for the numerical dispersion. This phenomenon occurs regardless the number $m + 1$ of conductors the

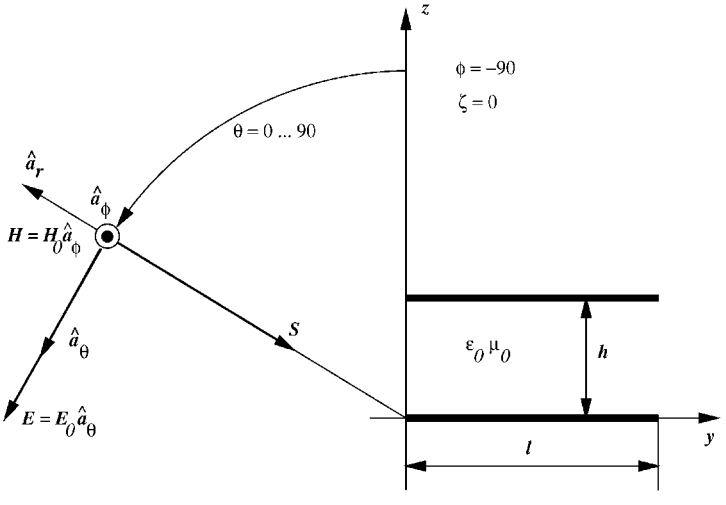

Figure 3. Transmission line used for numerical study.

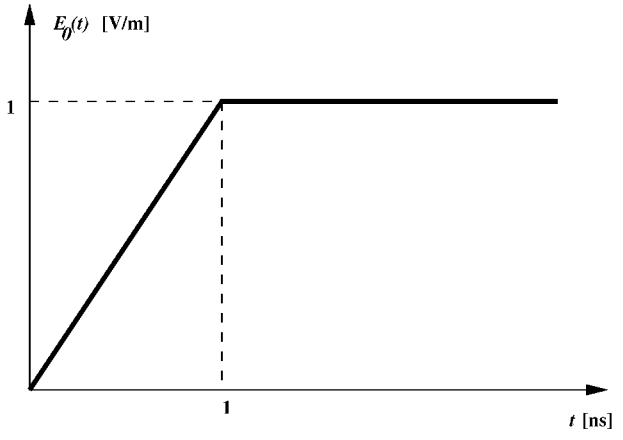

Figure 4. The waveform of the electric field.

transmission line contains or the presence/absence of a ground plane. Therefore, we present the results in the simplest case, that is a two-conductor lossless transmission line in free space, with no ground plane in its proximity.

The transmission line is made of two wires of radius $r_w = 10$ mils and length $l = 1$ m, which are parallel to the y-axis and placed at a distance $h = 2$ cm from each other, as shown in Figure 3. In this configuration the PUL parameters of the transmission line are given by

$$C = \frac{\pi \varepsilon_o}{\log\left(\dfrac{h}{r_w}\right)}$$
$$L = \frac{\mu_o \varepsilon_o}{C} \tag{21}$$

and they evaluate to $C = 6.3621$ (pF m^{-1}) and $L = 1.7465$ (μH m^{-1}).

In the numerical experiments, the angle θ was varied from 0 to 90°, while maintaining $\phi = -90°$ and $\zeta = 0°$. The waveform used for the electric field is shown in Figure 4.

The frequency content of the waveform is well below 1 GHz (i.e. the wavelength $\ll$ cross-section of the transmission line). According to the theory, both the AA and FTD models should produce accurate results but, as will be seen, the discrete DFTD counterpart of FTD model produces some numerical oscillations which, we believe, are due to the neglect of the phase term in the approximation given by (16).

For the particular problem considered here, we have

$$\mathbf{V}_f(t, y) = \left(\frac{v_y}{v_z} e_z - e_y\right) E_o(t, y, v_z h/v_o^2) \qquad \mathbf{V}_f(t, y) = \left(\frac{v_y}{v_z} e_z - e_y\right) \frac{v_z h}{v_o^2} \frac{\partial}{\partial t} E_o(t - v_y y/v_o^2)$$
$$\text{and} \tag{22}$$
$$\mathbf{I}_f(t, y) = -Ce_z \frac{v_o^2}{v_z} E_o(t, y, v_z h/v_o^2) \qquad \mathbf{I}_f(t, y) = -Ce_z h \frac{\partial}{\partial t} E_o(t - v_y y/v_o^2)$$

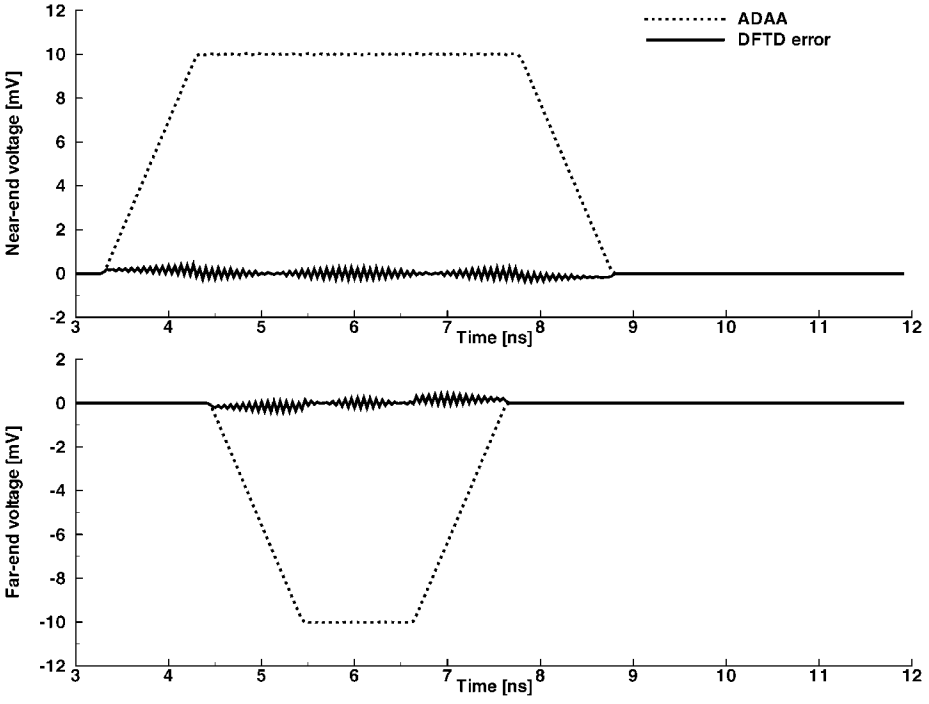

Figure 5. The error of the DFTD solution when the proper Δt, *i.e.* $\Delta t = g_j/v_0^2$, is used in the forcing function and when $\theta = 20^\circ$.

as forcing functions of the AA and FTD models, respectively. Based on (19), Δt in (18) should be varied as a function of θ as

$$\Delta t(\theta) = \frac{h}{v_o} \cos\theta \tag{23}$$

in order to obtain the exact AA forcing functions for the FTD model. A simulation example for such a substitution of Δt in (18), that is (17), is shown in Figure 5, which depicts the corresponding ADAA solution, which is assumed to be accurate, and the deviation of DFTD (17) solution from it.

In the numerical examples the $l = 1$ m long transmission line is discretized using 100 equal length intervals, hence $\Delta y = 1$ cm. The finite difference scheme (9) itself produces the minimum amount of numerical dispersion if run at its *Courant* limit. Therefore, since the maximum modal TEM propagation speed on our transmission line equals the speed of light $v_{\max} = c = 3 \times 10^8$ m s^{-1}, *at the Courant limit* $\Delta t = 33.(3)$ ps, hence resolving the rising edge of the pulse into a quite high number of $N_{\text{rising}} = 30$ intervals.

Just by substituting (19) into (17) one does not obtain total equivalence of the DAA and DFTD models, since the time instances in which the source field values are sampled are different in these two cases. In order to reach total equivalence, the discretization of (18)

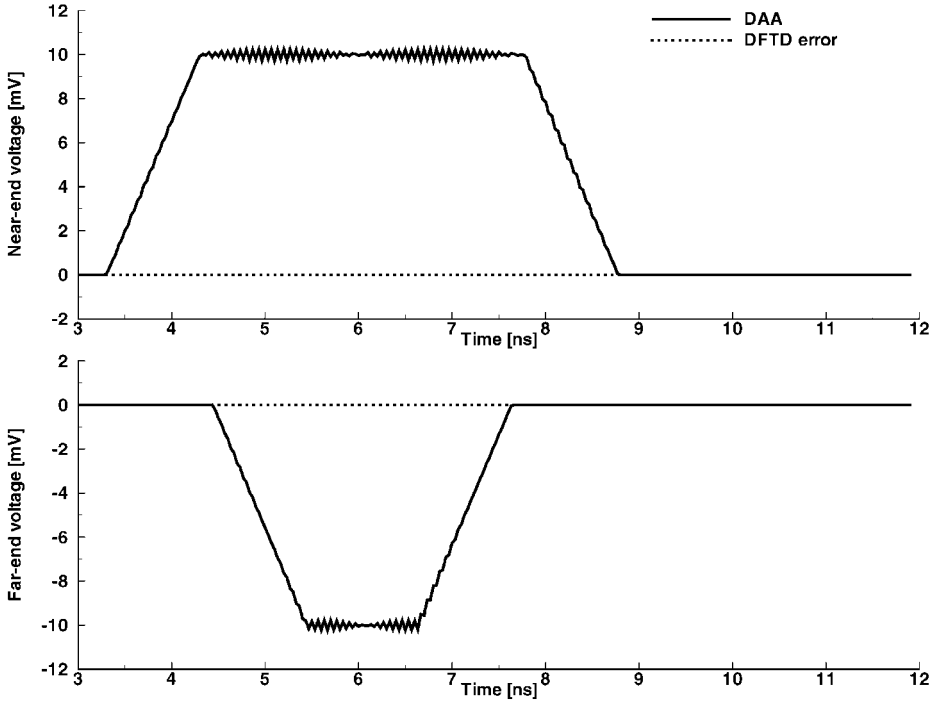

Figure 6. The error of the DFTD solution when $\Delta t = g_j/v_0^2$ and the source term is approximated by backwar differencing (DAA-DFTD equivalence study for $\theta = 20^\circ$).

has to be done by using backward differencing and not centred differencing as in (17). As Figure 6 shows, the difference between the non-averaged source using DAA and DFTD models disappears.

In Figures 7–10 comparative plots for various values of θ are shown. We note that the dispersion of the DFTD method varies with the angle θ, but it is not proportional to $\cos\theta$. For the most frequently studied cases, such as end-fire (Figure 7) or side-fire (Figure 10) excitation, most interestingly there is an insignificant numerical dispersion occurring in the DFTD method. The numerical dispersion can be minimal as for the case shown in Figure 9, or quite significant as for the case shown in Figure 8.

From Figures 7 and 10 it is clearly visible that some of the differences between the ADAA and DFTD models are due to the incorrect time instances the incident field is sampled in the case of the DFTD model. The 'DC' error in the rising and falling edges of the FTD solution gives a clear indication of this fact. Also, in these cases there are no oscillations around the solutions since the incident wave does not 'see' the cross-sectional dimension of the TL.

4. CORRECTION PROCEDURE FOR THE FTD METHOD

The amount of numerical dispersion generated by use of the DFTD formulation can be, in certain cases, completely eliminated by time averaging the discretized forcing

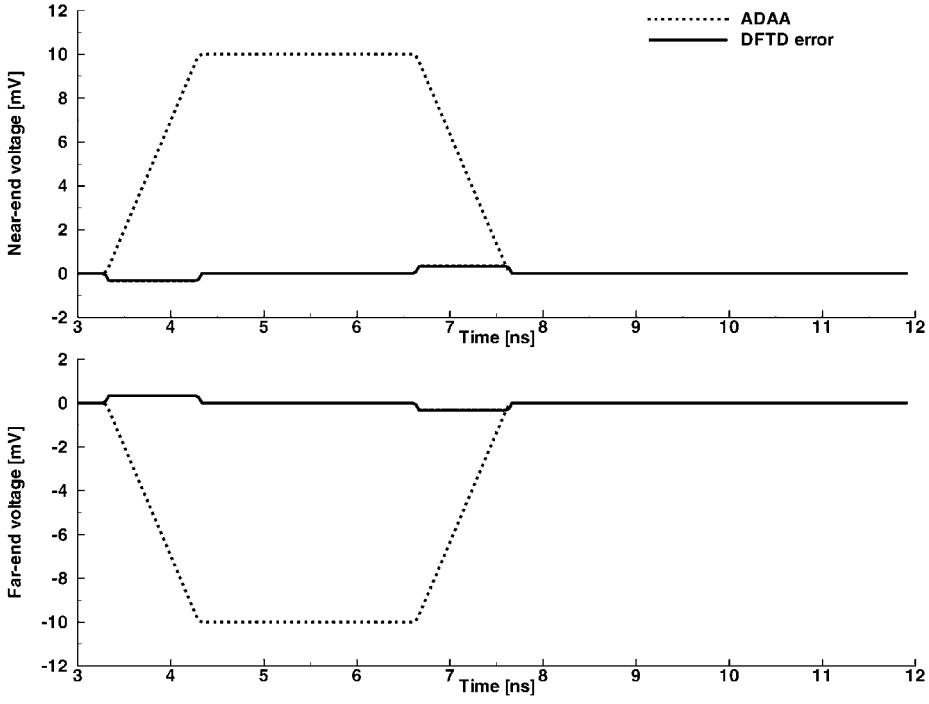

Figure 7. Comparison of the terminal voltages calculated by the two methods for $\theta = 0^\circ$ (end-fire case).

functions (17):

$$[\mathbf{V}_\mathrm{f}]_{k+1/2}^{n} = \begin{bmatrix} \cdots \\ \left(\dfrac{f_j}{g_j} v_y - e_y\right) \dfrac{g_j}{v_\mathrm{o}^2} \\ \cdots \end{bmatrix} \frac{[E_\mathrm{a}]_{k+1/2}^{n+1} - [E_\mathrm{a}]_{k+1/2}^{n-1}}{2\Delta t}$$

$$[\mathbf{I}_\mathrm{f}]_{k}^{n+1/2} = -C \begin{bmatrix} \cdots \\ f_j \\ \cdots \end{bmatrix} \frac{[E_\mathrm{a}]_{k}^{n+3/2} - [E_\mathrm{a}]_{k}^{n-1/2}}{2\Delta t} \tag{24}$$

Comparing (17) and (24) one can easily see that there is no increase in the computational cost of the time varying terms of the forcing functions, hence the algorithm can be as efficient as the original DFTD scheme. On the other hand, in some cases the form of the field may not be known via an analytic formula, that is it may be calculated using its own time-stepping procedure, and then the use of this new improved version of the DFTD scheme would require more storage since the field is needed a full time step ahead and behind the current update time.

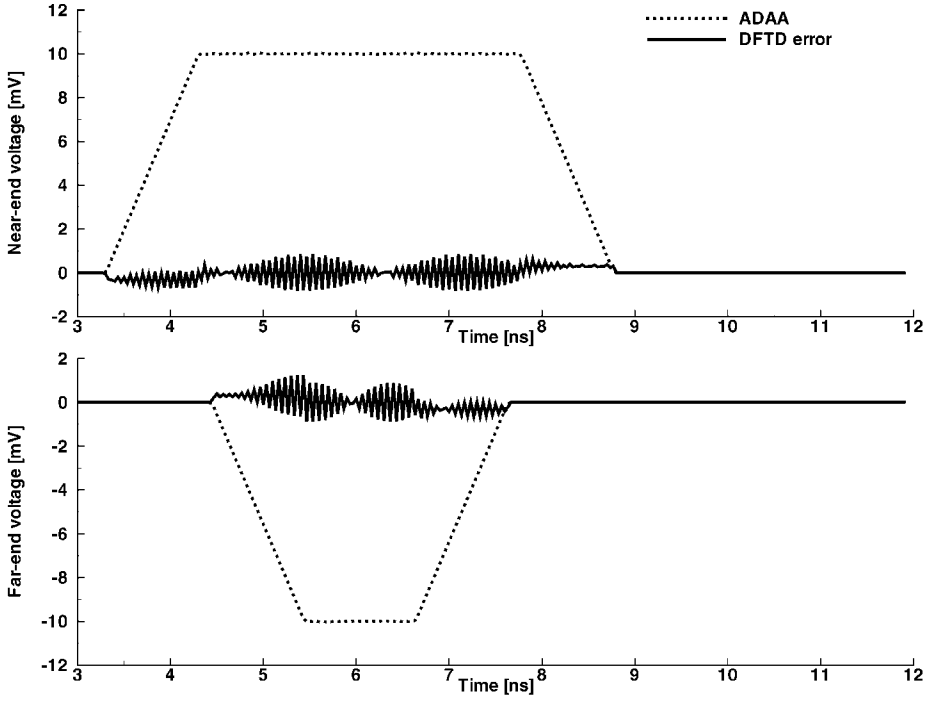

Figure 8. Comparison of the terminal voltages calculated by the two methods for $\theta = 20^{\circ}$.

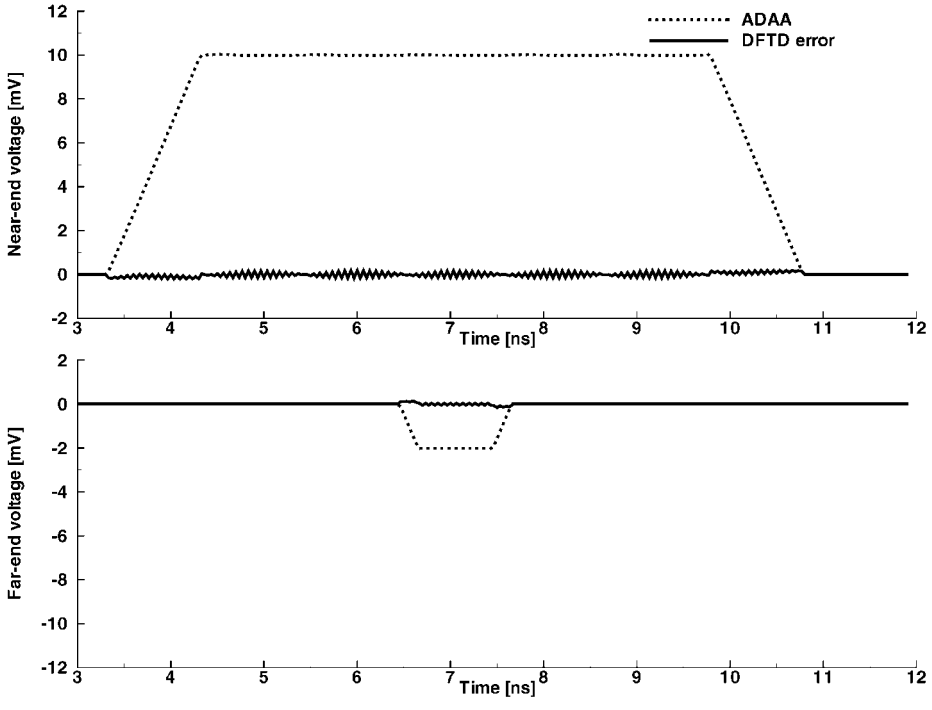

Figure 9. Comparison of the terminal voltages calculated by the two methods for $\theta = 70^{\circ}$.

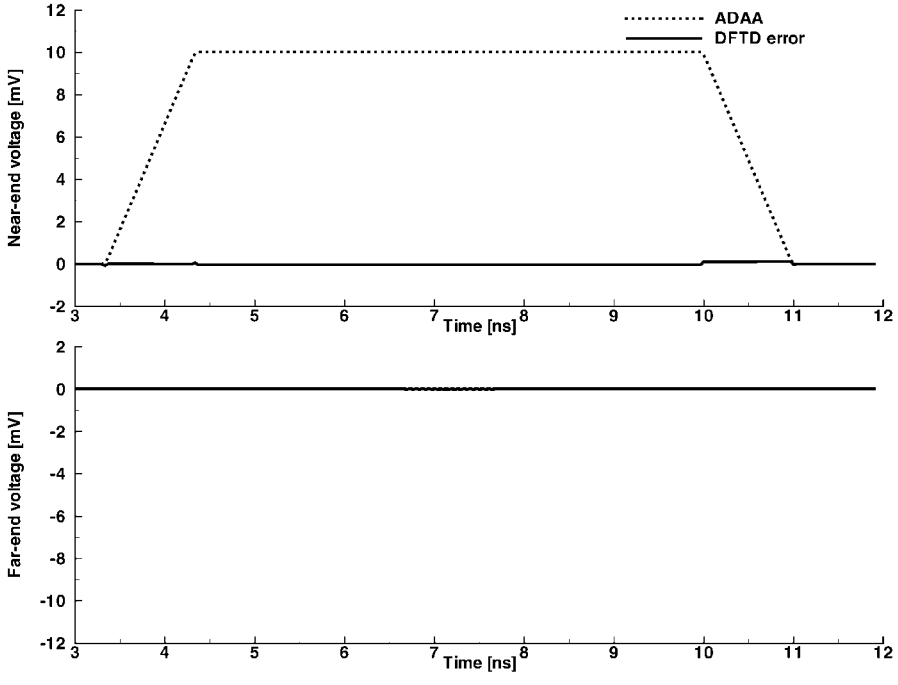

Figure 10. Comparison of the terminal voltages calculated by the two methods for $\theta = 90^\circ$ (side-fire case).

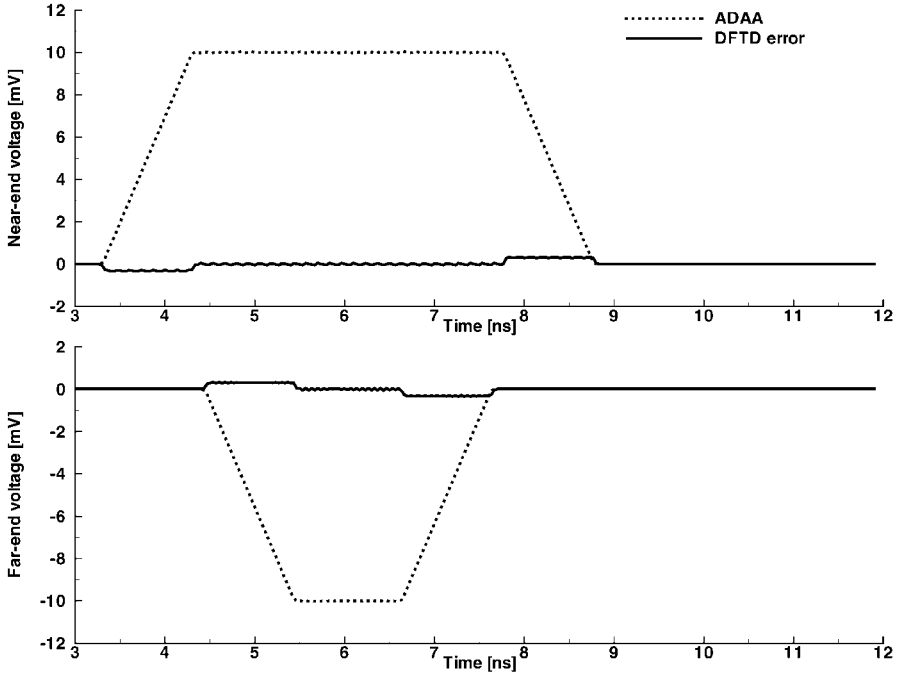

Figure 11. The error in the solution of the DFTD model with averaged source terms.

The improvement in the simulation results is displayed in Figure 11. Since the result is presented for one of the worst cases ($\theta = 20^\circ$), compared to Figure 8, the indicated improvement is quite significant. For other angles of incidence the improvement is at least as good as for $\theta = 20^\circ$.

Although the high-frequency oscillations are damped, the previously mentioned 'DC' error persists, which was expected, since the averaging by itself does not solve the problem of appropriate field sampling in the source terms.

5. CONCLUSIONS

Two models of external field coupling to MTLs have been compared. It has been shown that the mathematical approximations of the field coupling phenomena in case of the FTD model lead to un-predicted numerical error. Simulation results have been compared to the predictions of the computationally less efficient but more accurate AA model. It has been shown that time averaging of the forcing terms in the FTD model reduces significantly the numerical errors at no extra computational cost.

REFERENCES

1. Paul CR. *Analysis of Multiconductor Transmission Lines*. Wiley Series in Microwave and Optical Engineering. Wiley: New York, 1994.
2. Taylor CD, Satterwhite RS, Harrison Jr CW. The response of a terminated two wire transmission line excited by a nonuniform electromagnetic field. *IEEE Transactions on Antennas and Propagation* 1965; **13**(11):987–989.
3. Agrawal AK, Price HJ, Gurbaxani SH. Transient response of multiconductor transmission lines excited by a nonuniform electromagnetic field. *IEEE Transactions on Electromagnetic Compatibility* 1980; **22**(2).
4. Rachidi F. Formulation of field to transmission line coupling equations in terms of magnetic excitation. *IEEE Transactions on Electromagnetic Compatibility* 1993; **35**(3):404–407.
5. Mardare D, LoVetri J. The finite-difference time-domain solution of lossy MTL networks with nonlinear junctions. *IEEE Transactions on Electromagnetic Compatibility* 1995; **37**(2):252–259.
6. Lapohos T, LoVetri J, Seregelyi J. Experimental validation of models for external field coupling to MTL networks with nonlinear junctions. *1997 IEEE AP-S International Symposium and URSI North American Radio Science Meeting*, URSI Abstracts, Montréal, Canada, 13–18 July 1997; 137.
7. Lapohos T, LoVetri J, Seregelyi J. External field coupling to MTL networks with non-linear junctions: numerical modeling and experimental validation. *IEEE Transactions on Electromagnetic Compatibility* 2000; **42**(1):16–29.
8. Cangellaris AC. Distributed equivalent sources for the analysis of multiconductor transmission lines excited by an electromagnetic field. *IEEE Transactions on Microwave Theory and Techniques* 1988; **36**(10):1445–1448.
9. Bernardi P, Cicchetti R. Response of a planar microstrip line excited by an external electromagnetic field. *IEEE Transactions on Electromagnetic Compatibility* 1990; **32**(2):98–105.
10. Podosenov SA, Sokolov AA. Linear two-wire transmission line coupling to an external electromagnetic field. Part I: Theory. *IEEE Transactions on Electromagnetic Compatibility* 1995; **37**(4):559–566.
11. Podosenov SA, Sakharov KYu, Svekis YaG, Sokolov AA. Linear two-wire transmission line coupling to an external electromagnetic field. Part II: specific cases, experiment. *IEEE Transactions on Electromagnetic Compatibility* 1995; **37**(4):566–574.
12. Maio I, Canavero FG, Dilecce B. Analysis of crosstalk and field coupling to lossy MTLs in a SPICE environment. *IEEE Transactions on Electromagnetic Compatibility* 1996; **38**(3):221–229.
13. Celik M, Cangellaris CA, Yaghmour A. An all-purpose transmission-line model for interconnect simulation in SPICE. *IEEE Transactions on Microwave Theory and Techniques* 1997; **45**(10):1857–1867.
14. Lapohos T. Multiconductor transmission line networks. *Ph.D. Thesis*, The University of Western Ontario, London, Ontario, Canada, April 1998.

AUTHORS' BIOGRAPHIES

Tibor Lapohos (September 93–March 98) was born in Tîrgu-Mures, Romania, in 1967. He received the Electrical Engineering degree from the Department of Automation and Computer Technology of the Polytechnic University of Cluj-Napoca, Romania, in 1991. He received the MESc and PhD degrees from the University of Western Ontario in 1994 and 1998, respectively. In 1998 he joined the Electronic Countermeasures Section of the Defence Research Establishment Ottawa, Canada, as defence scientist. His main areas of interest are in wide-band sensors, time-domain measurements, electromagnetic compatibility problems and time-domain numerical methods.

Joe LoVetri was born in Enna, Italy, in 1963. He received the BSc (with distinction) and MSc degrees, both in Electrical Engineering, from the University of Manitoba in 1984 and 1987, respectively. From 1984 to 1986 he was EMI/EMC engineer at Sperry Defence Division in Winnipeg, Manitoba. From 1986 to 1988 he held the position of TEMPEST engineer at the Communications Security Establishment in Ottawa. From 1988 to 1991 he was a Research Officer at the Institute for Information Technology of the National Research Council of Canada. He received the PhD degree in Electrical Engineering from the University of Ottawa in 1991. From 1991 to 1999 he was an Associate Professor in the Department of Electrical and Computer Engineering at the University of Western Ontario. In 1997/98 he spent a sabbatical year at the TNO Physics and Electronics Laboratory in the Netherlands. He is currently with the Department of Electrical and Computer Engineering at the University of Manitoba. His main interests lie in time-domain computational electromagnetics, modelling of electromagnetic compatibility problems, ground penetrating radar and wideband identification techniques.